ADVANCED FUNCTIONAL MATERIALS
www.afm-journal.de

www.MaterialsViews.com

Influence of the Electron Deficient Co-Monomer on the Optoelectronic Properties and Photovoltaic Performance of Dithienogermole-based Co-Polymers

Chin Pang Yau, Zhuping Fei, Raja Shahid Ashraf, Munazza Shahid, Scott E. Watkins, Pichaya Pattanasattayavong, Thomas D. Anthopoulos, Vasilis G. Gregoriou, Christos L. Chochos,* and Martin Heeney**

A series of donor–acceptor (D–A) conjugated polymers utilizing 4,4-bis(2-ethylhexyl)-4*H*-germolo[3,2-*b*:4,5-*b*′]dithiophene (DTG) as the electron rich unit and three electron withdrawing units of varying strength, namely 2-octyl-2*H*-benzo[*d*][1,2,3]triazole (BTz), 5,6-difluorobenzo[*c*][1,2,5]thiadiazole (DFBT) and [1,2,5]thiadiazolo[3,4-*c*]pyridine (PT) are reported. It is demonstrated how the choice of the acceptor unit (BTz, DFBT, PT) influences the relative positions of the energy levels, the intramolecular transition energy (ICT), the optical band gap (E_g^{opt}), and the structural conformation of the DTG-based co-polymers. Moreover, the photovoltaic performance of poly[(4,4-bis(2-ethylhexyl)-4*H*-germolo[3,2-*b*:4,5-*b*′]dithiophen-2-yl)-([1,2,5]thiadiazolo[3,4-*c*]pyridine)] (PDTG-PT), poly[(4,4-bis(2-ethylhexyl)-4*H*-germolo[3,2-*b*:4,5-*b*′]dithiophen-2-yl)-(2-octyl-2*H*-benzo[*d*][1,2,3]triazole)] (PDTG-BTz), and poly[(4,4-bis(2-ethylhexyl)-4*H*-germolo[3,2-*b*:4,5-*b*′]dithiophen-2-yl)-(5,6-difluorobenzo[*c*][1,2,5]thiadiazole)] (PDTG-DFBT) is studied in blends with [6,6]-phenyl-C_{70}-butyric acid methyl ester ($PC_{70}BM$). The highest power conversion efficiency (PCE) is obtained by PDTG-PT (5.2%) in normal architecture. The PCE of PDTG-PT is further improved to 6.6% when the device architecture is modified from normal to inverted. Therefore, PDTG-PT is an ideal candidate for application in tandem solar cells configuration due to its high efficiency at very low band gaps ($E_g^{opt} = 1.32$ eV). Finally, the 6.6% PCE is the highest reported for all the co-polymers containing bridged bithiophenes with 5-member fused rings in the central core and possessing an E_g^{opt} below 1.4 eV.

1. Introduction

The development of low band gap polymers for organic photovoltaic devices (OPV) or transistor applications has progressed rapidly over the last decade. In the area of photovoltaics, a particularly successful strategy has been the donor–acceptor approach, in which an electron rich donor is co-polymerized with an electron deficient acceptor. The co-polymerization has shown to assist the reduction of the band gap by molecular orbital hybridization.[1–5] Computational density functional theory (DFT) calculations on donor–acceptor co-polymers have typically shown that the HOMO is delocalized over the conjugated backbone whilst the LUMO is more strongly localized on the acceptor co-monomer.[6–8] Therefore, tuning of either the electron rich or electron deficient unit is an effective method to engineer the band gap and energetic levels of the resulting co-polymers.

Electron rich bridged bithiophenes with 5-member fused rings in the central core such as 4*H*-cyclopenta[1,2-*b*:5,4-*b*′]dithiophene (**CPDT**), 4*H*-silolo[3,2-*b*:4,5-*b*′]dithiophene (**DTS**), and 4*H*-germolo[3,2-*b*:4,5-*b*′]dithiophene (**DTG**) have been shown to provide high performance electron donor polymers when co-polymerized with electron deficient moieties such as benzo[*c*][1,2,5]thiadiazole (**BT**).[9–13] Previously, we have reported the synthesis of high molecular weight **PDTG-BT** and demonstrated PCE of 4.5% in OPV devices with promisingly high short circuit currents (J_{sc}) of 18.6 mA cm^{-2} after annealing.[13] At the same period of time, other groups have also reported the synthesis of lower molecular weight **PDTG-BT** that exhibits somewhat

C. P. Yau, Dr. Z. Fei, Dr. R. S. Ashraf, Dr. M. Shahid, Dr. M. Heeney
Department of Chemistry and Centre for Plastic Electronics, Imperial College London
Exhibition Road, South Kensington, London, SW7 2AY, UK
E-mail: z.fei@imperial.ac.uk; m.heeney@imperial.ac.uk
Dr. S. E. Watkins
CSIRO Molecular and Health Technologies
VIC 3169, Australia

P. Pattanasattayavong, Prof. T. D. Anthopoulos
Department of Physics and Centre for Plastic Electronics
Imperial College London, Exhibition Road
South Kensington, London, SW7 2AY, UK
Dr. V. G. Gregoriou, Dr. C. L. Chochos
Advent Technologies SA
Patras Science Park, Stadiou Street
Platani-Rio, 26504, Patra, Greece
E-mail: cchochos@advent-energy.com

DOI: 10.1002/adfm.201302270

lower device efficiency.[14,15] Moreover, co-polymerization of **DTG** with different electron withdrawing groups,[16,17] such as 5-octyl-4*H*-thieno[3,4-*c*]pyrrole-4,6(5*H*)-dione (**TPD**) provide polymers with PCE of 7.4%[17] with a lower J_{sc} of 13.0 mA cm^{-2} but with an increased V_{oc} of 0.87 V as compared to **PDTG-BT**.[13] Interestingly, the performance of some **DTG** based-polymers in OPV devices has shown an increase in the PCE compared to that of the analogous carbon or silicon bridged alternatives.[18,19] This effect has been attributed to the increase in carbon-germanium bond length compared to the carbon-carbon or carbon-silicon bonds in **CPDT** and **DTS** respectively.[19] The increase in bond length has been suggested to result in a reduction of steric hindrance between the solubilizing group on the bridging heteroatom and adjacent co-monomers, which facilitates crystallization and close π–π stacking of the polymers. A similar behavior was earlier reported for polymers containing silicon bridging atoms versus their carbon bridged analogues.[11,12]

The encouraging results reported for **DTG** co-polymers have prompted this study into alternative electron-deficient building blocks in **DTG** based-polymers, with the aim to investigate how the optoelectronic properties and device performance vary as a function of acceptor strength. For comparison purposes, we investigated three structural analogues of **BT**, namely 5,6-difluorobenzo[*c*][1,2,5]thiadiazole (**DFBT**), [1,2,5]thiadiazolo[3,4-*c*]pyridine (**PT**), and 2-octyl-2*H*-benzo[*d*][1,2,3]triazole (**BTz**).[20–23] Here, we report the synthesis, characterization and device properties of all three co-polymers (**PDTG-BTz**, **PDTG-DFBT**, **PDTG-PT**), and compare their performance to previously reported **BT** co-polymer.[13] We observe significant differences in optoelectronic properties and device performance and relate these to the nature of the acceptor co-monomer.

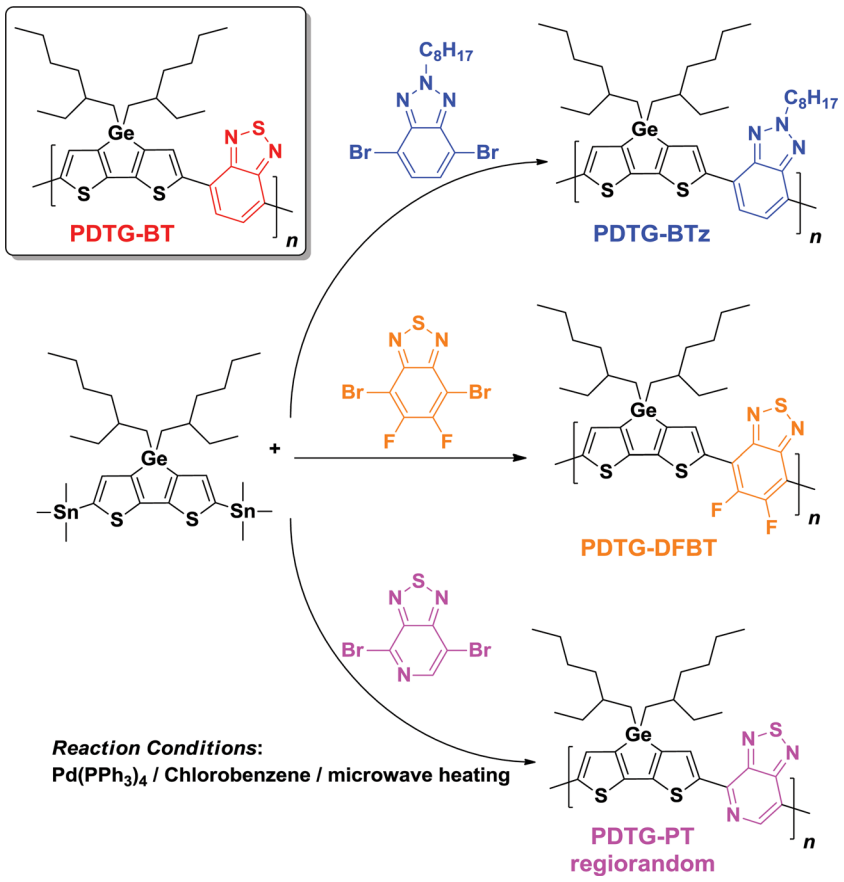

Scheme 1. Synthetic route to **PDTG-BTz**, **PDTG-DFBT**, and (Regiorandom) **PDTG-PT**. In the inset the chemical structure of **PDTG-BT** is presented.

2. Results and Discussion

2.1. Synthesis

4,4-Bis(2-ethylhexyl)-2,6-bis(trimethylstannyl)-4*H*-germolo[3,2-*b*:4,5-*b*′]dithiophene (**DTG-Sn$_2$**),[19] 4,7-dibromo-2-octyl-2*H*-benzo[*d*][1,2,3]triazole,[24] 4,7-Dibromo-[1,2,5] thiadiazolo[3,4-*c*] pyridine,[21,25] and 4,7-dibromo-5,6-difluorobenzo[*c*][1,2,5] thiadiazole,[26] were all synthesized according to the previously reported literature. However, purification of **DTG-Sn$_2$** was complicated due to the fact that the monomer was non-crystalline. Attempted purification over silica or alumina resulted in extensive de-stannylation as previously noted.[19] Therefore, preparative GPC was utilized to give high purity monomer in 59% yield. All polymers were synthesized using microwave assisted Stille cross coupling polymerization reactions as shown in **Scheme 1** and purified by sequential Soxhlet extraction with methanol, acetone, and hexane to remove low molecular weight oligomers and catalyst residues.[27] In the case of **PDTG-BTz** and **PDTG-PT**, both polymers were readily soluble in chloroform but the crude polymers were both relatively low molecular weights ($M_n \approx 7$ kDa). Since it is known that OPV device performance usually improves using higher molecular weight polymers,[28–31] high molecular weight fractions with low polydispersity were isolated using preparative GPC in chlorobenzene.[32] For **PDTG-DFBT**, we found that the crude product was poorly soluble in both chloroform and chlorobenzene, precluding preparative GPC. The reduced solubility of polymer containing the **DFBT** co-monomer has previously been reported by other groups, and may be related to intra and intermolecular sulfur–fluorine interactions.[33,34] Therefore extraction of the crude **PDTG-DFBT** with hot chlorobenzene resulted in isolation of a soluble fraction of low molecular weight. However, the majority of the yield was insoluble material. Molecular weights were measured by gel permeation chromatography (GPC) against polystyrene standards and are summarized in **Table 1**. In the case of the **PDTG-DFBT**, the poor solubility of the polymer at higher molecular weights resulted in the use of the low molecular weight fraction in this study. The molecular

Table 1. Summary of polymer physical properties.

	M_n [kDa][a)]	M_w [kDa][a)]	PDI	DP	λ_{max} (sol) [nm]	λ_{max} (film) [nm]
PDTG-BTz	23	27	1.16	33	575, 616	585, 626
PDTG-DFBT	8	11	1.51	13	677, 735	675, 739
PDTG-PT	24	33	1.36	38	773, 831	784, 848

[a)]Determined by GPC and reported as their polystyrene equivalents.

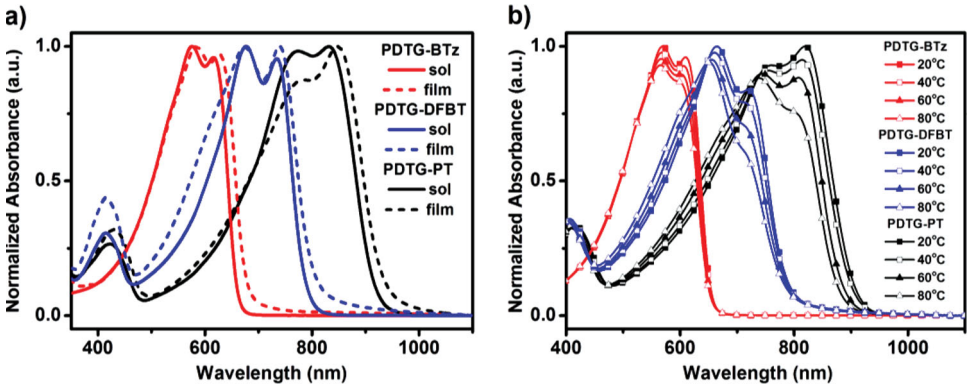

Figure 1. a) UV-Vis spectrum of polymers in solution (CB) and film, b) temperature UV studies in solution (CB).

weights of **PDTG-PT** and **PDTG-BTz** were quite similar and all three polymers have relatively low polydispersity (PDI) indexes.

The ^{1}H NMR of all three polymers (see Supporting Information) was consistent with their proposed structures. However, whilst **PDTG-BTz** exhibited a clear spectrum with sharp peaks, both **PDTG-PT** and **PDTG-DFBT** exhibited relatively broad featureless peaks in common with many other low band gap polymers. We attribute this broadening to the segmental aggregation of the polymer in solution and the presence of a variety of chain conformations which cannot freely rotate. The enhanced peak broadening for the lower band gap polymers may be due to the increased double bond character between the co-monomer units due to the lower lying LUMO energy levels and enhanced quinoidal character of the backbone. Enhanced quinoidal character would reduce free rotation in the backbone. In the case of **PDTG-PT**, we note that the synthesis route used may provide a mixture of regioisomers for the relative orientation of the [1,2,5] thiadiazolo[3,4-*c*]pyridine. It has previously been shown that the 2-position of the [1,2,5]thiadiazolo[3,4-*c*]pyridine (ortho to the pyridyl nitrogen) undergoes oxidative coupling more rapidly than the 5 position, which may lead to some enhancement in the percentage of regioregularity versus the purely random co-polymer.[35–38] However in our case the broad ^{1}H NMR spectra prevented further analysis of their regioregularity.

2.2. Optical and Electrochemical Properties

The normalized UV-Vis absorption spectra of co-polymers **PDTG-BTz**, **PDTG-DFBT**, and **PDTG-PT** in chlorobenzene solution and as thin films are presented in **Figure 1**, and the corresponding optoelectronic properties are summarized in Table 1. All polymers display qualitatively similar spectral shape in the long wavelength region, with pronounced double peaks apparent in both solution and solid state (Figure 1a). Upon film formation the longer wavelength peak increases in intensity relative to solution and slightly red-shifts indicative of enhanced interchain interactions. The similarity between the solution and thin film absorption spectra at the higher wavelengths suggests that the polymers may be aggregating in solution at room temperature. Indeed as shown in Figure 1b, heating the solutions results in a significant decrease in intensity of the longer wavelength shoulder in all cases, as well as a slight blue shift of the absorption. Heating most likely increases torsional disorder in the backbone, disrupting the planarity of the polymers and decreasing their tendency to aggregate. Note the effect is less pronounced for **PDTG-BTz** than for other two co-polymers, in agreement with the solution state ^{1}H NMR data. Based on this observation, the peaks of **PDTG-BTz**, **PDTG-DFBT**, and **PDTG-PT** at 575 nm, 677 nm, and 773 nm, respectively in solution can be assigned to the intramolecular D–A charge transfer (ICT) interactions,[39,40] whereas the peaks at 616 nm, 735 nm, and 831 nm are attributed to the aggregated form of the co-polymers. Consequently, the peaks of the alternating dithienogermole-benzothiadiazole co-polymer (**PDTG-BT**), reported in our previous work,[13] at 700 nm and 756 nm in solution can safely be assigned to the D–A ICT interactions and aggregate form, respectively.

Passing from solution to the solid state, a similar behavior is also presented by studying the absorption spectra of **PDTG-BTz**, **PDTG-DFBT** and **PDTG-PT** (Figure 1a). In more detail, **PDTG-BTz** shows maxima at 585 nm with a shoulder at 626 nm, the **PDTG-DFBT** exhibits maxima at 739 nm with a shoulder at 675 nm and **PDTG-PT** reveals maxima at 848 nm

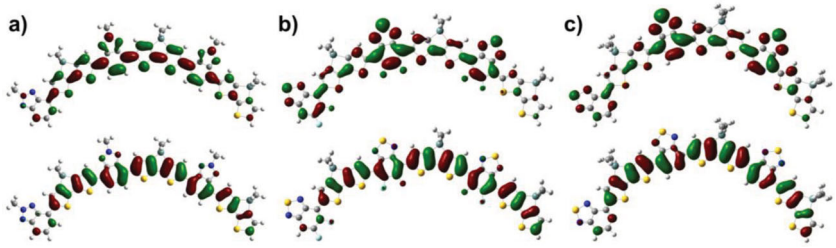

Figure 2. DFT (B3LYP/6-31G*) calculated frontier molecular orbitals of the HOMO (bottom) and LUMO (top) for the trimers of a) **PDTG-BTz**, b) **PDTG-DFBT**, and c) **PDTG-PT**.

with a shoulder at 784 nm. It should be noted that **PDTG-BT** display maxima at 778 nm with a shoulder at 714 nm.[13] Based on the assignment reported previously for the peaks of the co-polymers in solution, the peaks of **PDTG-BTz**, **PDTG-BT**, **PDTG-DFBT**, and **PDTG-PT** at 585 nm, 714 nm, 675 nm, and 784 nm, respectively are related to the ICT interactions and those at 626 nm, 778 nm, 739 nm, and 848 nm to the aggregated form.

Interestingly, the variations in the ICT transitions of our co-polymers do not strictly follow[3] the commonly observed trend reported in the literature that the stronger the electron accepting nature and quinoid forming ability of the electron deficient unit, the stronger the intramolecular charge transfer and lower the E_g^{opt}.[21,41] The energy gap of the intramolecular charge transfer of the DTG-based co-polymers follows the order: **PDTG-BTz** > **PDTG-DFBT** > **PDTG-BT** > **PDTG-PT** whilst the electron accepting strength of the electron deficient monomer follows the order: **PT** > **DFBT** > **BT** > **BTz**.[42] We rule out any differences in torsional disorder between **BT** and **DFBT** being the cause for this increase in band gap, since DFT calculations of the conjugated backbone (vide infra) suggest that the **DFBT** co-polymer is able to adopt a completely co-planar backbone despite the slightly larger size of fluorine compared to hydrogen (**Figure 2**). Similarly, we do not believe the lower molecular weight of **PDTG-DFBT** is responsible for the increase in band gap, since no differences in the optical absorption spectra of similarly low weight **PDTG-BT** versus higher molecular weight polymer were apparent.[14] In addition highly dilute solution spectra of the 'insoluble' higher weight fraction of **PDTG-DFBT** in tetrachloroethane also show no appreciable differences to the more soluble lower weight fraction, suggesting the effective conjugation length is reached in the soluble fraction. We note others have observed a similar increase in band gap upon the exchange of **BT** with **DFBT** in donor–acceptor co-polymers,[7,26,34,43] and in agreement with these results ascribe the increase in band gap to the electron withdrawing influence of the two fluorine atoms on the HOMO energy level of **PDTG-DFBT**. Finally, the optical band gaps, as measured by the onset of UV-Vis absorption in the solid state are 1.82 eV (680 nm) for **PDTG-BTz**, 1.53 eV (810 nm) for **PDTG-DFBT**, 1.32 eV (940 nm) for **PDTG-PT**, and 1.47 eV (843 nm) for **PDTG-BT.**

In comparing the effect of the germanium bridging group, it is useful to compare the properties of the present polymers to those of the previously reported analogous polymers incorporating bridging C or Si atoms with identical 2-ethylhexyl solubilizing groups. Thus, for example, the poorly soluble **DFBT** co-polymer with 4*H*-cyclopenta[1,2-*b*:5,4-*b′*]dithiophene (**CPDT**) shows a similar dual peak spectra, with the longer wavelength aggregation peaks absorbing at 712 nm in chloroform solution and 761 nm as a thin film, and with a band gap of 1.6 eV.[44] The **BTz** co-polymer with 4*H*-silolo[3,2-*b*:4,5-*b′*]dithiophene (**DTS**) exhibits a less pronounced dual peak absorption and has a maximum absorption of 567 nm in chloroform and 576 nm in thin film, with an optical band gap of 1.8 eV.[45] Thus, replacement of the bridging Ge for Si appears to have a relatively minor influence of the optical properties in agreement with other studies,[19,46] whereas replacing the Ge with C appears to slightly red-shift the maximum absorption.

The ionization potential of **PDTG-BTz**, **PDTG-DFBT**, and **PDTG-PT** polymer thin films was measured by photo-electron spectroscopy in air (PESA) to be –4.75 eV, –5.0 eV, and –4.9 eV respectively. From the direct measurements of the HOMO, we can approximate the LUMO levels by subtracting the optical band gap, to obtain values of –2.95 eV, –3.6 eV, and –3.6 eV for **PDTG-BTz**, **PDTG-DFBT**, and **PDTG-PT**, respectively as shown in **Table 2**. For comparative purposes the ionization of **PDTG-BT** measured by the same technique is –4.8 eV, with a corresponding LUMO level of –3.3 eV.[13] From these results, it is evident that the replacement of the **BT** monomer with **DFBT** or **PT** shifts both the HOMO and LUMO levels to lower values due to the stronger electron accepting properties of both **DFBT** and **PT**. Comparing the HOMO and LUMO energy levels of **PDTG-DFBT** and **PDTG-PT** it can be seen that while the two co-polymers reveal similar LUMO levels, the HOMO of **PDTG-DFBT** is lying deeper than that of **PDTG-PT** in accordance with other examples in the literature[20,23] and verifying the assumption that the fluorine atoms on the **DFBT** unit have a significant electron withdrawing effect. Finally, the replacement of the **BT** with **BTz** results in an upshifted LUMO level for **PDTG-BTz** due to the

Table 2. Comparison of experimental and calculated HOMO, LUMO, and Band Gap.

	HOMO [eV][a)]	LUMO [eV][b)]	Optical E_g [eV][c)]	Calc. HOMO [eV]	Calc. LUMO [eV]	Calc. E_g [eV]
PDTG-BTz	–4.75 ± 0.05	–2.95 ± 0.05	1.82	–4.50	–2.62	1.88
PDTG-DFBT	–5.00 ± 0.05	–3.6 ± 0.05	1.53	–4.80	–3.20	1.60
PDTG-PT	–4.90 ± 0.05	–3.6 ± 0.05	1.32	–4.79	–3.33	1.46

[a)]Determined as a thin film by UV-PESA; [b)]Estimated by the subtraction of the optical band gap from the HOMO; [c)] Determined by onset of optical absorption.

weaker electron accepting properties of **BTz** as compared to **BT**, but the HOMO levels of the co-polymers are almost similar.

Quantum chemical (DFT) calculations were performed to predict the molecular energy levels and model the distribution of the frontier molecular orbitals of the co-polymers (Figure 2). Trimer model compounds were modeled using Gaussian 09 at the B3LYP/6-31G* level. The side chains were modified to methyl groups in order to simplify the calculations. The minimum-energy conformations of the trimers reveal that all have essentially a planar backbone conformation, with little differences in torsional disorder between them. The calculated HOMO-LUMO energy gaps of the trimers show reasonable correlation to the experimentally observed values (Table 2), with the same trend between materials observed. Moreover, even though the predicted HOMO levels are somewhat upshifted to that observed experimentally, they follow a broadly similar trend with the exception of **PDTG-PT**, which is predicted to have a similar HOMO level to **PDTG-DFBT**. These differences may be due to solid state packing effects for the actual polymer films, which are not taken into account on the DFT calculations. From the molecular orbital diagrams in Figure 2, it is possible to observe that in all three materials the HOMO is fully delocalized along the polymer chain axis. However, distinct differences are observed in the case of the LUMO, which we relate to the strength of the electron deficient unit. For example both **PDTG-PT** and **PDTG-DFBT** show a significant localization of the LUMO around the electron deficient acceptor units compared to **DTG** in the backbone. However, **PDTG-BTz** shows comparatively less localization around the **BTz** unit and a LUMO which is more delocalized over the backbone of the trimer. The differences in the LUMO localization correlate well with the strength of the ICT interaction, with a stronger interaction observed for the more strongly localized LUMOs.

2.3. Structural (X-Ray) Characterization

The ordering of thin films of the polymers was investigated by wide angle X-ray scattering (WAXS). Films were prepared by drop casting from chlorobenzene at room temperature. As shown in **Figure 3**, for both **PDTG-PT** and **PDTG-DFBT** there is clear diffraction peak present at 5.16° and 4.94° (2θ) corresponding to d-spacings of 17.11 nm and 17.91 nm respectively, which we attribute to the lamellar packing of the polymer backbones.[47,48] Both polymers are similar to the 17.6 nm spacing observed for **PDTG-BT**.[13] In contrast, there is no peak present for **PDTG-BTz** which indicates a more amorphous structure. We believe this may be due to the extra octyl side chain present on the **BTz** monomer which may hinder lamellar packing by preventing intercalation of the solubilizing chains. In addition, this octyl side chain initially protrudes in the same plane as the conjugated backbone, whereas the side chains on the germanium bridge protrude perpendicular to the conjugated backbone. This particular combination of in and out of plane solubilizing groups appears to frustrate the ordering of the polymer. There is a broad and weak diffraction peak around at 25.4° (2θ) for **PDTG-PT** corresponding to a d-space packing of 3.5 nm, which we attribute to π–π stacking distance, similar to that observed in **PDTG-BT**. This peak is considerably broader and less intense in **PDTG-DFBT** but occurs in a similar region whilst it appears to be absent altogether for **PDTG-BTz** in agreement with its amorphous character.

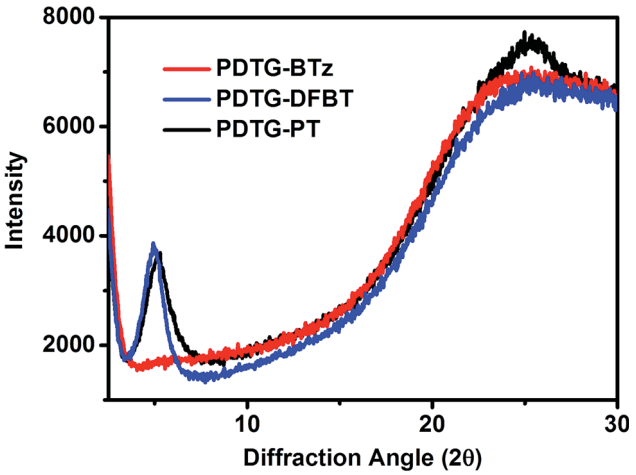

Figure 3. X-Ray diffraction patterns of **PDTG-PT**, **PDTG-BTz**, and **PDTG-DFBT** films drop cast from chlorobenzene.

2.4. Photovoltaic Properties

Initial photovoltaic devices were prepared using a glass|ITO|PEDOT:PSS|Polymer:Fullerene-Blend|LiF|Al device structure, measured under 100 mW cm^{-2} AM 1.5 illumination and averaged over at least five devices. Varying polymer:fullerene blends of ratios (1:2 wt%) prepared from 1,2-dichlorobenzene were screened. **$PC_{70}BM$** was used to complement the polymers by capturing the low wavelength region. Their respective J–V curves and device properties can be seen in **Figure 4**a and **Table 3**. The highest PCE of 4.6% was achieved by **PDTG-PT**, while the PCE of **PDTG-BTz** and **PDTG-DFBT** were 2.4% and 2.1%, respectively.

Previously, we have reported **PDTG-BT** to provide high J_{sc} (18.4 mA cm^{-2}) after device optimization but low V_{oc} (0.56 V) and FF (0.42), limiting the overall PCE to 4.5%.[13] All three polymers investigated here show an increase in the V_{oc} compared to **PDTG-BT**. For both **PDTG-DFBT** and **PDTG-PT**, the increment in V_{oc} is in agreement with the experimentally observed increased ionization potentials relative to **PDTG-BT**, and can be related to the increase in energy gap between the polymer HOMO and the **$PC_{70}BM$** LUMO.[49–51] Surprisingly, the highest recorded V_{oc} was obtained by **PDTG-BTz**-based devices despite the fact that both experimental and computational results demonstrated that **PDTG-BTz** has the smallest ionization potential amongst the studied materials. The analogous Si bridged polymer, **PDTS-BTz**, also exhibits a similarly high voltage of 0.71 V, but lower overall efficiencies.[45] We are unclear of the exact reasons for this, but believe it may be partly due to differences in the molecular packing of the pristine polymer film and the blend film. Although **PDTG-BTz** appears largely amorphous by WAXS, the optical spectra clearly indicate it has a marked tendency to aggregate in solution and the solid state. Incorporation of the fullerene may disrupt this

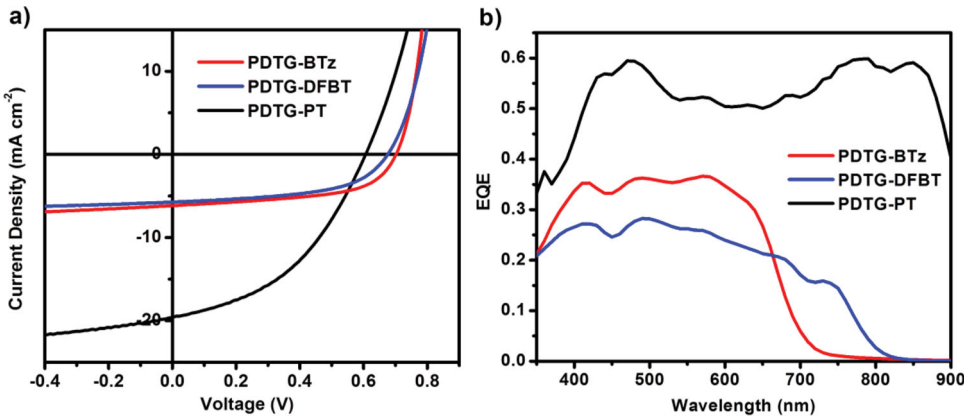

Figure 4. a) *J–V* curves and b) EQE of polymer solar cells based on Polymer:**$PC_{70}BM$** blends (1:2 wt%) without solvent additives.

aggregation and increase disorder in the blend film, resulting in a reduction of the effective conjugation length along the polymer backbone and therefore an increase in the effective ionization potential. The **PDTG-BTz** may be more prone to the effects of disorder than the other two polymers due to the higher lying LUMO level which corresponds to reduced quinoidal character of the conjugated backbone, in agreement with the solution ^{1}H NMR results. High quinoidal character is associated with increasing double bond character between the two co-monomer units, and therefore a more rigid co-planar backbone, which is less prone to torsional disorder. We note that an increase in polymer ionization potential has been observed for **P3HT** upon blending due to the effects of disorder.[52] In our case, PESA measurements were also performed upon the blended films (see Supporting Information, Figure S10). For both **PDTG-PT** and **PDTG-DFBT**, no differences were observed in the measured ionization potential for the pristine and blend films. However, for **PDTG-BTz** a small increase in ionization potential of 0.05 eV was consistently observed for the blend film. Whilst not sufficient to fully account the increase in open circuit voltage, in combination with other factors such as changes in charge recombination dynamics, they partly explain the anomalous open circuit voltage.

Amongst the three co-polymers, only **PDTG-PT** has a J_{sc} and PCE comparable to that of **PDTG-BT**. **PDTG-BTz**, and **PDTG-DFBT** both show a large decrease in the J_{sc}. For **PDTG-BTz** this could be attributed to the relatively narrow absorption range and increased band gap. For **PDTG-DFBT** the optical band gap (1.53 eV) is similar to **PDTG-BT**, so we believe the reduced performance is principally due to the lower molecular weight of the polymer. We note in the case of **PDTG-BT**, low molecular weight polymers have shown significantly lower photocurrents in blends with **$PC_{70}BM$**.[14,15] We further note that during the preparation of this manuscript Ohshita and co-workers have reported a **PDTG-PT** with a M_n of 6.2 kDa.[53] The UV-Vis spectra from this polymer showed a marked reduction in the long wavelength shoulder which is usually attributed to aggregation, compared to our data for the higher molecular weight polymer. Their OPV devices were fabricated in a similar manner and showed V_{oc} of 0.57 V, J_{sc} of 8.89 mA cm^{-2}, FF of 0.57 and overall PCEs of 2.9%. Again, the difference in molecular weight appears to have a large effect on the efficiency, predominately though a reduction in the J_{sc}. Examination of the EQE data (Figure 4b) shows a broad photocurrent generation into the longer wavelengths for the **PDTG-PT** analogue with an approximate 50–60% EQE over the absorption window, whereas both the **PDTG-BTz** and the **PDTG-DFBT** give a much lower 20% and 35% over a smaller EQE wavelength range. The EQE spectra mirror the optical absorption spectra in all three cases. Particularly significant is the charge generation out to 900 nm in the case of **PDTG-PT** due to its very low band gap of 1.32 eV allowing it to absorb more photons in the NIR region. Thus, **PDTG-PT** is one of the few co-polymers[30,54,55] with E_g^{opt} below 1.4 eV that exhibits such a high EQE at longer wavelengths.

Table 3. Summary of the short circuit current (J_{sc}), open circuit voltage (V_{oc}), fill factor (FF) and power conversion efficiency (PCE) of OPV devices.

Polymer:$PC_{70}BM$ (1:2) in oDCB	J_{SC} [mA cm^{-2}]	V_{oc} [V]	FF	PCE [%]
PDTG-BTz	6.17	0.70	0.56	2.4
PDTG-DFBT	5.74	0.67	0.54	2.1
PDTG-PT	17.7	0.61	0.43	4.6
PDTG-PT +5 vol% DMF	17.5	0.60	0.44	4.6
PDTG-PT + 3 vol% CN	18.7	0.61	0.43	4.9
PDTG-PT + 2.5 vol% DIO	17.6	0.59	0.50	5.2

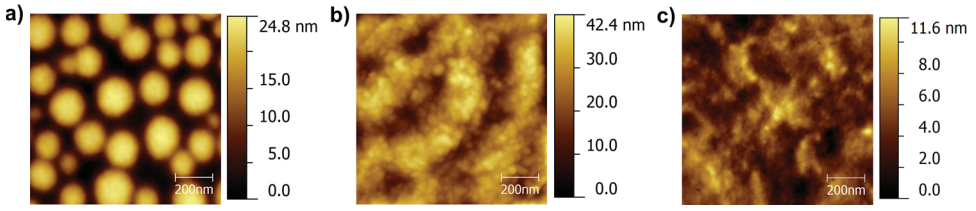

Figure 5. AFM topography of **a) PDTG-BTz/$PC_{70}BM$**, **b) PDTG-DFBT/$PC_{70}BM$**, and **c) PDTG-PT/$PC_{70}BM$** films.

2.5. Thin Film Morphology

As mentioned above, the PCEs of the **PDTG-BTz/$PC_{70}BM$** and **PDTG-DFBT/$PC_{70}BM$** devices were limited by the low J_{sc} (6.17 and 5.74 mA cm^{-2}). As J_{sc} is partly determined by charge recombination, which can be correlated to nanoscale morphology, atomic force microscopy (AFM) topography was performed to probe the surface of the devices. **Figure 5** shows the topography of all three polymer-fullerene blends spun into films directly onto PEDOT:PSS. Large differences in surface morphology are clearly observed between the three blends. In the case of **PDTG-BTz/$PC_{70}BM$** blend films, rather large features on the order of 100–200 nm are apparent, with a root mean square (RMS) surface roughness of 6.70 nm. Such large domains are suggestive of poor intermixing between the polymer and fullerene and are generally considering non-optimal for good device performance.[56–59] The high alkyl chain density of **PDTG-BTz** in comparison to the other co-polymers may lead to the poor intermixing of fullerene in this case, hampering intercalation of the fullerene between the conjugated polymer backbones. Blends of **PDTG-DFBT** also show relatively large features on the order of 20–40 nm, and films with appreciable surface roughness (RMS of 6.77 nm). Here, the poor solubility of the polymer and its high propensity to aggregate in solution may be inhibiting effective mixing with **$PC_{70}BM$**. Blends of **PDTG-PT/$PC_{70}BM$** showed much finer mixing in addition to the lowest surface roughness (RMS of 1.78 nm). The good intermixing can help to explain the increased J_{sc} simply by increasing the interfacial area for charge separation.

2.6. PDTG-PT Optimizations

The promising initial performance of **PDTG-PT** prompted us to further investigate the use of processing additives to further enhance performance, with the particular aim of further improving the rather low fill factor of the as-spun films. Three solvents additives were investigated, dimethylformamide (DMF),[60] 1-chloronaphthalene (CN)[61] and 1,8-diiodooctane (DIO)[62] in different volumetric ratios. The *J–V* characteristics of devices fabricated from 1:2 polymer:**$PC_{70}BM$** solutions are shown in supporting information. While no significant improvement in the PCE was recorded with the use of DMF and CN (Table 3) the use of 2.5 vol% DIO afforded a modest increase in the overall PCE from 4.61% to 5.2% mainly as a result of an increase in fill factor, with J_{sc} = 17.6 mA cm^{-2}, V_{oc} = 0.58 V, and FF = 0.51.

Recent work has demonstrated the ability of the **PT** monomer to accept a Lewis acid through complexation of the nitrogen lone pair.[63,64] This coordination or complexation induces a reduction in both the HOMO and LUMO but it is more pronounced on the LUMO energy, thus lowering the band gap. As PEDOT:PSS is inherently acidic, the normal device structure may be limiting the full potential of the **PDTG-PT:$PC_{70}BM$** system. Indeed, a recent study by Olsen, Bazan, and co-workers, upon a small molecule electron donor containing **PT**, demonstrated that removing the acidic hole injection layers and replace them with a solution processable nickel oxide injection layer resulted in a significant enhancement in device performance.[65] Therefore, we were interested to investigate the potential of **PDTG-PT** in an inverted device architecture in which molybdenum oxide (MoO_3) was used as the interface layer.

The inverted structure consisted of a glass/ITO/ZnO (≈30 nm)/Active layer/MoO_3 (10 nm)/Ag (100 nm) configuration. Active layers were fabricated from the highest performing solutions containing 2.5 vol% DIO in 1,2-dichlorobenzene. The ZnO was produced by the sol gel method[66] and both the MoO_3 and silver were thermally evaporated. Comparisons of the device characteristics and EQE, for both the normal and inverted cells, are shown in **Figure 6** and the data summarized in **Table 4**. When comparing the normal and inverted device there is an increase in overall PCE from 5.2% to 6.6%. Both the normal and inverted devices exhibit identical V_{oc} of 0.59 V. However the inverted device exhibits a significantly enhanced photocurrent, from 17.6 to 19.6 mA cm^{-2}, and fill factor from 0.51 to 0.57 respectively. Observing the *J–V* curve, it is evident that there is a significant increase in the shunt resistance of the inverted device. This increase in shunt resistance is typically associated with the reduction of leakage current and has been linked with: less leakage at the edge of the device, fewer pinholes in the film and fewer trapping sites.[67,68] Similarly, the boost in the photocurrent for the inverted device may result from a number of effects, including changes in the vertical segregation of the active film layer, improved optical interference effects as a result of changes in the optical field density within the active layer or improved extraction of charges from the use of different hole and electron transporting layers. In addition the removal of PEDOT:PSS, which has a small but significant absorption in the near-IR region, may also enhance the active layer absorption in the near-IR region. The EQE shows a general increase over the 650–900 nm range from approximately 55% to 60% resulting in an increase in overall current. This trend has also been observed by Reynolds and co-workers using the PDTG-TPD in normal and inverted device structure.[19,69] Overall, the use of an inverted device structure increased the efficiency by 1.4%.

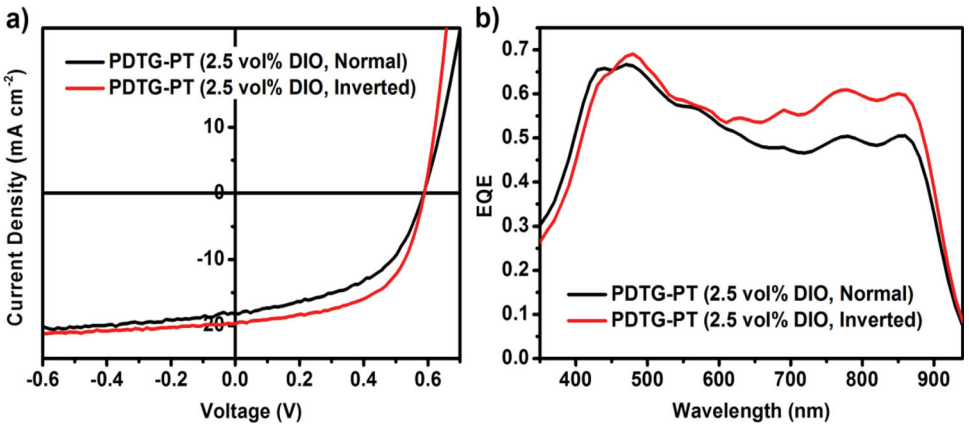

Figure 6. a) *J–V* curves and b) EQEs of **PDTG-PT:PC$_{70}$BM** (1:2) with 2.5 vol% DIO in both normal and inverted devices.

Table 4. Summary of the photovoltaic parameters and power conversion efficiency of normal and inverted **PDTG-PT** Devices.

PDTG-PT:PC$_{70}$BM (1:2) in oDCB 2.5 vol% DIO	J_{sc} [mA cm^{-2}]	V_{oc} [V]	FF	PCE [%]
Normal	17.6	0.59	0.50	5.2
Inverted	19.6	0.59	0.57	6.6

3. Conclusions

The development of three new **DTG**-based co-polymers utilizing Stille cross-coupling polymerization was demonstrated. In addition, an extensive structure-optoelectronic properties-device performance relationship studies has been performed using spectroscopic and morphological (structural) analysis techniques (UV-Vis, PESA, AFM, and XRD) as well as OPV device fabrication. Comparing the impact of the electron deficient unit on the optoelectronic properties of the co-polymers, it is important to note the discrepancy between the strength of the acceptor and the ICT energy gap. Among the three co-polymers (**PDTG-BTz**, **PDTG-DFBT**, **PDTG-PT**), the **PDTG-PT** has shown similar device characteristics to that of **PDTG-BT** but with an improved V_{oc}, increasing the overall PCE of the OPV device. **PDTG-PT** performed relatively well with or without additive which may be due to better mixing with **PC$_{70}$BM** and the high EQE at long wavelengths. An inverted device structure was used to further enhance the performance of **PDTG-PT** to 6.6%. Thus, **PDTG-PT** is an ideal candidate for application in tandem solar cells configuration due to its high efficiency at very low band gaps (E_g^{opt} = 1.32 eV), while the 6.6% PCE is the highest reported for all the co-polymers containing bridged bithiophenes with 5-member fused rings in the central core and possessing an E_g^{opt} below 1.4 eV.

4. Experimental Section

All reactions were treated as air and light sensitive and performed under argon and in the dark. All glassware used were washed using teepol surfactant, rinsing with excess water, acetone and methylene dichloride and dried in an oven at 120 °C. All solvents and reagents were sourced commercially from Aldrich. The synthesis of 4,7-dibromo-[1,2,5]thiadiazolo[3,4-*c*]pyridine, 4,7-dibromo-5,6-difluorobenzo[*c*][1,2,5]thiadiazole, 4,7-dibromo-2-octyl-2*H*-benzo[*d*][1,2,3]triazole and 4,4-bis(2-ethylhexyl)-2,6-bis(trimethylstannyl)-4*H*-germolo[3,2-*b*:4,5-*b*′]dithiophene was performed according to the previously reported literature.[19,21,24–26] ^{1}H and ^{13}C NMR spectra were recorded on a Bruker AV-400 (400 MHz for ^{1}H and 100 MHz for ^{13}C), using the residual solvent resonance of $CDCl_3$ as an internal reference. Number-average (M_n) and weight-average (M_w) molecular weight were determined by Agilent Technologies 1200 series GPC running in chlorobenzene at 80 °C, using two PL mixed columns in series and calibrated against narrow polydispersity polystyrene standards. Electrospray mass spectrometry was performed with a Thermo Electron Corporation DSQII mass spectrometer. UV-Vis spectra were recorded on a UV-1601 Shimadzu UV-Vis spectrometer. Flash chromatography (FC) was performed on silica gel (Merck Kieselgel 60 F254 230–400 mesh). A customer build Shimadzu recSEC system was used to fractionate the polymers and purify the tin monomer. The system comprises a DGU-20A3 degasser, an LC-20A pump, a CTO-20A column oven, an Agilent PLgel 10 µm MIXED-D column and a SPD-20A UV detector. Polymers were fractionated using chlorobenzene as eluent at 80 °C. Monomers were purified on an identical system using running in hexane at 40 °C. Photo electron spectroscopy in air (PESA) measurements were recorded with a Riken Keiki AC-2 PESA spectrometer with a power setting of 5 nW and a power number of 0.5. Samples for PESA were prepared on glass substrates by spin coating. Data reported is the average of 3 separate thin film measurements for pristine samples, and 2 films for blend samples. X-ray diffraction (XRD) measurements were performed on the PANALYTICAL X′ PERT-PRO MRD diffractometer equipped with nickel-filtered Cu Kα1 beam and X′ CELERATOR detector, using current I = 40 mA and accelerating voltage V = 40 kV. Samples were prepared by drop casting.

The conventional devices were fabricated using the structure of Glass/ITO/PEDOT:PSS (30–40 nm)/active layer (80–90 nm)/LiF (1 nm)/Al (100 nm). In case of inverted device architecture it was Glass/ITO/ZnO (≈30 nm)/active layer (80–90 nm)/MoO_3(10 nm)/Ag (100 nm). Indium tin oxide (ITO) coated glass was first cleaned using via sequential sonication in detergent (Mucasol), water (DI), acetone and finally isopropanol. 30–40 nm of poly(ethylenedioxythiophene):poly(styrenesulfonate) (PEDOT:PSS, Baytron P TP AI 4083, Bayer AG) was then deposited via spin coating and dried at 150 °C for 20 min. Additives and n-type material were added to a 12 mg mL^{-1} polymer solution and stirred overnight. The following blend solution was then spin coated to a thickness of approximately 80–90 nm. LiF (1 nm) was then thermally deposited followed by Al (120 nm) under high vacuum (10^{-6} mbar). The device area was 0.045 cm^2 in both cases.

OPVs were characterized using a Xenon lamp at AM1.5 solar illumination (Oriel 300 W solar simulator). Incident photon conversion efficiency (IPCE) measurements were made using a 100 W tungsten halogen lamp (Bentham IL1 with Bentham 605 stabilized current power supply) coupled to a monochromator and a computer-controlled stepper motor (Bentham M300, 300 mm focal length, slit width 3.7 nm, 1800 lines m^{-1} grating). The photon flux of light incident to the samples was calibrated using a UV-enhanced silicon photodiode. A 590 nm long-pass glass filter was inserted into the beam at illumination wavelengths longer than 620 nm to remove light from second-order diffraction. Photocurrent was measured using a Keithley 2400 source meter; Measurement duration for a given wavelength was sufficient to ensure the current had stabilized (up to around 5 s under low or zero bias light conditions). All electrical measurements of OPVs were executed in the inert N_2 purged devices chamber.

Poly[(4,4-bis(2-ethylhexyl)-4H-germolo[3,2-b:4,5-b′]dithiophen-2-yl)-([1,2,5]thiadiazolo[3,4-c]pyridine)](PDTG-PT): 4,4-Bis(2-ethylhexyl)-2,6-bis(trimethylstannyl)-4*H*-germolo[3,2-*b*:4,5-*b′*]dithiophene (1.010 g, 1.28 mmol) was weighed into a pre-dried microwave vial. 4,7-Dibromo-[1,2,5]thiadiazolo[3,4-*c*]pyridine (377 mg, 1.28 mmol) and $Pd(PPh_3)_4$ (37 mg, 0.032 mmol) were added. The microwave vial was capped and degassed with argon and vacuum (×3). Chlorobenzene (9 mL) was added and the mixture further degassed with stirring for 30 min. The resulting solution was then heated in the microwave reactor (constant heating mode) at 100 °C (2 min), 120 °C (5 min), 140 °C (5 min), 160 °C (5 min), and 180 °C (40 min). The reaction was cooled to 50 °C and then precipitated into methanol before filtering into a cellulose thimble. Lower molecular weight fractions were removed via Soxhlet extraction with methanol (1 day), acetone (1 day), hexane (1 day), and extracted with chloroform (3 h) before being concentrated and dried under vacuum. The mass before fractionation was 492.5 mg (yield 61%). The polymer was then subjected to fractionation using preparative GPC (eluent: chlorobenzene). Fractions of similar molecular weights were combined and concentrated under reduced pressure, followed by precipitation into methanol to afford a black solid (56.5 mg, 7% yield). ^{1}H NMR (400 MHz, $CDCl_3$, 40 °C) δ 8.95 – 7.75 (m, 3H), 2.04 – 0.74 (m, 34H). GPC (Chlorobenzene, 80 °C) M_n = 24 000 g mol^{-1}, M_w = 33 000 g mol^{-1}.

Poly[(4,4-bis(2-ethylhexyl)-4H-germolo[3,2-b:4,5-b′]dithiophen-2-yl)-(2-octyl-2H-benzo[d][1,2,3]triazole)] (PDTG-BTz): Following the method reported above, 4,4-bis(2-ethylhexyl)-2,6-bis(trimethylstannyl)-4*H*-germolo[3,2-*b*:4,5-*b′*]dithiophene (302.3 mg, 0.383 mmol), 4,7-dibromo-2-octyl-2*H*-benzo[*d*][1,2,3]triazole (149 mg, 0.383 mmol), chlorobenzene (2 mL) and $Pd(PPh_3)_4$ (11.1 mg 9.58 µmol) were reacted together. Following work-up and precipitation, impurities, and oligomers of the crude polymer were removed via Soxhlet extraction with methanol (1 day), acetone (1 day), hexane (1 day), and extracted with chloroform (3 h). The polymer from the chloroform fraction was then subjected to fractionation using preparative GPC (eluent: chlorobenzene). Fractions of similar molecular weights were combined and, solutions were then concentrated down under reduced pressure, followed by precipitation into methanol to afford a black solid (42.1 mg, 15% yield). ^{1}H NMR (400 MHz, $CDCl_3$, δ) 8.16 (s, 2H), 7.67 (s, 2H), 4.89 (s, 2H), 2.29 (s, 2H), 1.66 (s, 2H), 1.55 – 1.23 (m, 30H), 0.89 (m, 15H). GPC (Chlorobenzene, 80 °C) M_n = 23 000 g mol^{-1}, M_w = 27 000 g mol^{-1}.

Poly[(4,4-bis(2-ethylhexyl)-4H-germolo[3,2-b:4,5-b′]dithiophen-2-yl)-(5,6-difluorobenzo[c][1,2,5]thiadiazole)] (PDTG-DFBT): Following the method reported above, 4,4-bis(2-ethylhexyl)-2,6-bis(trimethylstannyl)-4*H*-germolo[3,2-*b*:4,5-*b′*]dithiophene (302.2 mg, 0.383 mmol), 4,7-dibromo-5,6-difluorobenzo[c][1,2,5]thiadiazole (126 mg, 0.383 mmol), chlorobenzene (2 mL) and $Pd(PPh_3)_4$ (11.1 mg 9.58 µmol) were reacted together. Following work-up and precipitation, impurities and oligomers of the crude polymer were removed via Soxhlet extraction with methanol (1 day), acetone (1 day), hexane (1 day) and chloroform (3 hour). Due to low solubility, the crude polymer was further extracted with chlorobenzene, most of the solvent removed and the solution precipitated into methanol to afford a black solid (36.3 mg, 15% yield). ^{1}H NMR (400 MHz, $CDCl_3$, δ) 8.39 (s, 2H), 2.01–0.74 (broad, 34H). GPC (Chlorobenzene, 80 °C) M_n = 8 000 g mol^{-1}, M_w = 11 000 g mol^{-1}.

Supporting Information

Supporting Information is available from the Wiley Online Library or from the author.

Acknowledgements

This work was supported by EPSRC grants EP/G060738/1, and EP/I002936/1. C.L.C. would like to thank the Ministry of Education and Religious Affairs in Greece for the financial support of this work provided under the co-operational program "AdvePol: E850". The authors would like to thank Ester Buchaca-Domingo for performing the WAXS experiments. The licence on this manuscript was changed on February 5, 2014.

Received: July 5, 2013
Revised: August 15, 2013
Published online: October 27, 2013

[1] S. Günes, H. Neugebauer, N. S. Sariciftci, *Chem. Rev.* **2007**, *107*, 1324.
[2] C. J. Brabec, M. Heeney, I. McCulloch, J. Nelson, *Chem. Soc. Rev.* **2011**, *40*, 1185.
[3] C. L. Chochos, S. A. Choulis, *Prog. Polym. Sci.* **2011**, *36*, 1326.
[4] C. Duan, F. Huang, Y. Cao, *J. Mater. Chem.* **2012**, *22*, 10416.
[5] A. Facchetti, *Chem. Mater.* **2011**, *23*, 733.
[6] C. Risko, M. D. McGehee, J. L. Brédas, *Chem. Sci.* **2011**, *2*, 1200.
[7] H. A. Bronstein, J. M. Frost, A. Hadipour, Y. Kim, C. B. Nielsen, R. S. Ashraf, B. P. Rand, S. Watkins, I. McCulloch, *Chem. Mater.* **2013**, *25*, 277.
[8] C. L. Chochos, A. Avgeropoulos, E. Lidorikis, *J. Chem. Phys.* **2013**, *138*, 064901.
[9] J. Hou, H. Y. Chen, S. Zhang, G. Li, Y. Yang, *J. Am. Chem. Soc.* **2008**, *130*, 16144.
[10] M. Morana, H. Azimi, G. Dennler, H. J. Egelhaaf, M. Scharber, K. Forberich, J. Hauch, R. Gaudiana, D. Waller, Z. Zhu, K. Hingerl, S. S. van Bavel, J. Loos, C. J. Brabec, *Adv. Funct. Mater.* **2010**, *20*, 1180.
[11] H. Y. Chen, J. Hou, A. E. Hayden, H. Yang, K. N. Houk, Y. Yang, *Adv. Mater.* **2010**, *22*, 371.
[12] M. C. Scharber, M. Koppe, J. Gao, F. Cordella, M. A. Loi, P. Denk, M. Morana, H. J. Egelhaaf, K. Forberich, G. Dennler, R. Gaudiana, D. Waller, Z. Zhu, X. Shi, C. J. Brabec, *Adv. Mater.* **2010**, *22*, 367.
[13] Z. Fei, J. S. Kim, J. Smith, E. B. Domingo, T. D. Anthopoulos, N. Stingelin, S. E. Watkins, J. S. Kim, M. Heeney, *J. Mater. Chem.* **2011**, *21*, 16257.
[14] J. Ohshita, Y. Y. Hwang, T. Mizumo, H. Yoshida, Y. Ooyama, Y. Harima, Y. Kunugi, *Organometallics* **2011**, *30*, 3233.
[15] D. Gendron, P. O. Morin, P. Berrouard, N. Allard, B. R. Aïch, C. N. Garon, Y. Tao, M. Leclerc, *Macromolecules* **2011**, *44*, 7188.
[16] Z. Fei, M. Shahid, N. Yaacobi-Gross, S. Rossbauer, H. Zhong, S. E. Watkins, T. D. Anthopoulos, M. Heeney, *Chem. Commun.* **2012**, *48*, 11130.
[17] C. E. Small, S. Chen, J. Subbiah, C. M. Amb, S. W. Tsang, T. H. Lai, J. R. Reynolds, F. So, *Nat. Photonics* **2012**, *6*, 115.
[18] J. S. Kim, Z. Fei, D. T. James, M. Heeney, J. S. Kim, *J. Mater. Chem.* **2012**, *22*, 9975.
[19] C. M. Amb, S. Chen, K. R. Graham, J. Subbiah, C. E. Small, F. So, J. R. Reynolds, *J. Am. Chem. Soc.* **2011**, *133*, 10062.
[20] H. Zhou, L. Yang, A. C. Stuart, S. C. Price, S. Liu, W. You, *Angew. Chem. Int. Ed.* **2011**, *50*, 2995.
[21] N. Blouin, A. Michaud, D. Gendron, S. Wakim, E. Blair, R. Neagu-Plesu, M. Belletête, G. Durocher, Y. Tao, M. Leclerc, *J. Am. Chem. Soc.* **2008**, *130*, 732.

[22] Z. Zhang, B. Peng, B. Liu, C. Pan, Y. Li, Y. He, K. Zhou, Y. Zou, *Polym. Chem.* **2010**, *1*, 1441.
[23] H. Zhou, L. Yang, S. C. Price, K. J. Knight, W. You, *Angew. Chem. Int. Ed.* **2010**, *49*, 7992.
[24] B. Peng, A. Najari, B. Liu, P. Berrouard, D. Gendron, Y. He, K. Zhou, Y. Zou, M. Leclerc, *Macromol. Chem. Phys.* **2010**, *211*, 2026.
[25] Y. Sun, S. C. Chien, H. L. Yip, Y. Zhang, K. S. Chen, D. F. Zeigler, F. C. Chen, B. Lin, A. K. Y. Y. Jen, *J. Mater. Chem.* **2011**, *21*, 13247.
[26] Y. Zhang, S. C. Chien, K. S. Chen, H. L. Yip, Y. Sun, J. A. Davies, F. C. Chen, A. K. Y. Jen, *Chem. Commun.* **2011**, *47*, 11026.
[27] S. Tierney, M. Heeney, I. McCulloch, *Synth. Met.* **2005**, *148*, 195.
[28] C. Müller, E. Wang, L. M. Andersson, K. Tvingstedt, Y. Zhou, M. R. Andersson, O. Inganäs, *Adv. Funct. Mater.* **2010**, *20*, 2124.
[29] T. Y. Chu, J. Lu, S. Beaupré, Y. Zhang, J. R. Pouliot, J. Zhou, A. Najari, M. Leclerc, Y. Tao, *Adv. Funct. Mater.* **2012**, *22*, 2345.
[30] L. Dou, C. C. Chen, K. Yoshimura, K. Ohya, W. H. Chang, J. Gao, Y. Liu, E. Richard, Y. Yang, *Macromolecules* **2013**, *46*, 3384.
[31] J. C. Bijleveld, A. P. Zoombelt, S. G. J. Mathijssen, M. M. Wienk, M. Turbiez, D. M. de Leeuw, R. A. J. Janssen, *J. Am. Chem. Soc.* **2009**, 16616.
[32] R. S. Ashraf, B. C. Schroeder, H. A. Bronstein, Z. Huang, S. Thomas, R. J. Kline, C. J. Brabec, P. Rannou, T. D. Anthopoulos, J. R. Durrant, I. McCulloch, *Adv. Mater.* **2013**, *25*, 2029.
[33] Z. Li, J. Lu, S. C. Tse, J. Zhou, X. Du, Y. Tao, J. Ding, *J. Mater. Chem.* **2011**, *21*, 3226.
[34] B. C. Schroeder, Z. Huang, R. S. Ashraf, J. Smith, P. D'Angelo, S. E. Watkins, T. D. Anthopoulos, J. R. Durrant, I. McCulloch, *Adv. Funct. Mater.* **2012**, *22*, 1663.
[35] S. T. Handy, T. Wilson, A. Muth, *J. Org. Chem.* **2007**, *72*, 8496.
[36] S. Schröter, C. Stock, T. Bach, *Tetrahedron* **2005**, *61*, 2245.
[37] J. Tilley, S. Zawoiski, *J. Org. Chem.* **1988**, 386.
[38] L. Ying, B. B. Y. Hsu, H. Zhan, G. C. Welch, P. Zalar, L. a Perez, E. J. Kramer, T. Q. Nguyen, A. J. Heeger, W. Y. Wong, G. C. Bazan, *J. Am. Chem. Soc.* **2011**, *133*, 18538.
[39] S. A. Jenekhe, L. Lu, M. M. Alam, *Macromolecules* **2001**, *34*, 7315.
[40] L. Biniek, C. L. Chochos, N. Leclerc, O. Boyron, S. Fall, P. Lévèque, T. Heiser, *J. Polym. Sci. A* **2012**, *50*, 1861.
[41] T. L. D. Tam, W. Ye, H. H. R. Tan, F. Zhou, H. Su, S. G. Mhaisalkar, A. C. Grimsdale, *J. Org. Chem.* **2012**, *77*, 10035.
[42] M. E. Köse, *J. Phys. Chem. A* **2012**, *116*, 12503.
[43] S. C. Price, A. C. Stuart, L. Yang, H. Zhou, W. You, *J. Am. Chem. Soc.* **2011**, *133*, 4625.
[44] Y. Li, J. Zou, H. L. Yip, C. Z. Li, Y. Zhang, C. C. Chueh, J. Intemann, Y. Xu, P. W. Liang, Y. Chen, A. K. Y. Jen, *Macromolecules* **2013**, *46*, 5497.
[45] J. Min, Z. Zhang, S. Zhang, M. Zhang, J. Zhang, Y. Li, *Macromolecules* **2011**, *44*, 7632.
[46] Z. Fei, Y. Kim, J. Smith, E. B. Domingo, N. Stingelin, M. A. McLachlan, K. Song, T. D. Anthopoulos, M. Heeney, *Macromolecules* **2011**, *45*, 735.
[47] A. Salleo, R. J. Kline, D. M. DeLongchamp, M. L. Chabinyc, *Adv. Mater.* **2010**, *22*, 3812.
[48] J. Rivnay, S. C. B. Mannsfeld, C. E. Miller, A. Salleo, M. F. Toney, *Chem. Rev.* **2012**, *112*, 5488.
[49] B. Rand, D. Burk, S. Forrest, *Phys. Rev. B.* **2007**, *75*, 115327.
[50] V. Chauhan, R. Hatton, P. Sullivan, T. Jones, S. W. Cho, L. Piper, A. DeMasi, K. Smith, *J. Mater. Chem.* **2010**, *20*, 1173.
[51] C. J. Brabec, A. Cravino, D. Meissner, N. S. Sariciftci, T. Fromherz, M. T. Rispens, L. Sanchez, J. C. Hummelen, *Adv. Funct. Mater.* **2001**, *11*, 374.
[52] T. M. Clarke, A. M. Ballantyne, J. Nelson, D. D. C. Bradley, J. R. Durrant, *Adv. Funct. Mater.* **2008**, *18*, 4029.
[53] J. Ohshita, M. Miyazaki, F. B. Zhang, D. Tanaka, Y. Morihara, *Polym. J.* **2013**, *45*, 979.
[54] L. Dou, W. H. Chang, J. Gao, C. C. Chen, J. You, Y. Yang, *Adv. Mater.* **2013**, *25*, 825.
[55] W. Li, K. H. Hendriks, W. S. C. Roelofs, Y. Kim, M. M. Wienk, R. A. J. Janssen, *Adv. Mater.* **2013**, *25*, 3182.
[56] D. Vacar, E. Maniloff, D. McBranch, A. J. Heeger, *Phys. Rev. B.* **1997**, *56*, 4573.
[57] X. Yang, J. Loos, *Macromolecules* **2007**, *40*, 1353.
[58] H. Hoppe, N. S. Sariciftci, *J. Mater. Chem.* **2006**, *16*, 45.
[59] P. E. Shaw, A. Ruseckas, I. D. W. Samuel, *Adv. Mater.* **2008**, *20*, 3516.
[60] T. Y. Chu, S. Alem, S. W. Tsang, S. C. Tse, S. Wakim, J. Lu, G. Dennler, D. Waller, R. Gaudiana, Y. Tao, *Appl. Phys. Lett.* **2011**, *98*, 253301.
[61] F. C. Chen, H. C. Tseng, C. J. Ko, *Appl. Phys. Lett.* **2008**, *92*, 103316.
[62] J. K. Lee, W. L. Ma, C. J. Brabec, J. Yuen, J. S. Moon, J. Y. Kim, K. Lee, G. C. Bazan, A. J. Heeger, *J. Am. Chem. Soc.* **2008**, *130*, 3619.
[63] H. Fukumoto, T. Yamamoto, *J. Polym. Sci. A* **2008**, *5*, 2975.
[64] G. C. Welch, G. C. Bazan, *J. Am. Chem. Soc.* **2011**, *133*, 4632.
[65] A. Garcia, G. C. Welch, E. L. Ratcliff, D. S. Ginley, G. C. Bazan, D. C. Olson, *Adv. Mater.* **2012**, *24*, 5368.
[66] H. Y. Park, D. Lim, K. D. Kim, S. Y. Jang, *J. Mater. Chem. A* **2013**, *1*, 6327.
[67] A. Savva, F. Petraki, P. Elefteriou, L. Sygellou, M. Voigt, M. Giannouli, S. Kennou, J. Nelson, D. D. C. Bradley, C. J. Brabec, S. A. Choulis, *Adv. Energy Mater.* **2013**, *3*, 391.
[68] B. Qi, J. Wang, *Phys. Chem. Chem. Phys.* **2013**, *15*, 8972.
[69] J. R. Manders, S. W. Tsang, M. J. Hartel, T. H. Lai, S. Chen, C. M. Amb, J. R. Reynolds, F. So, *Adv. Funct. Mater.* **2013**, *23*, 2993.